Int. J. Electrochem. Sci., 12 **(2017)** 6966 – 6979, doi: 10.20964/2017.08.26

International Journal of
ELECTROCHEMICAL
SCIENCE
www.electrochemsci.org

A Clean and Highly Efficient Leaching–Electrodeposition Lead Recovery Route in $HClO_4$ Solution

Xuan Zhang, Yanzhi Sun, Junqing Pan[*]

State Key Laboratory of Chemical Resource Engineering, Beijing University of Chemical Technology, Beijing 100029, China
[*]E-mail: jqpan@mail.buct.edu.cn

Received: 25 April 2017 / *Accepted:* 3 June 2017 / *Published:* 12 July 2017

To address a series of problems in the hydrometallurgical process of lead recovery, such as high energy consumption (810-930 kWh ton^{-1}), low efficiency and electrolyte pollution, we invented a novel, highly efficient and clean route for recovering high purity metallic lead via a leaching-electrodeposition process in a $HClO_4$ solution. First, the desulfurated spent lead paste and lead plate-grids from spent lead–acid batteries were dissolved in the $HClO_4$ solution to generate a $HClO_4$–$Pb(ClO_4)_2$ solution, denoted as the leaching process. An electrolysis process was then conducted in this solution to obtain metallic lead with $HClO_4$ regenerated for reuse in the next batch, denoted as the electrodeposition process. For the leaching process, the concentration of $HClO_4$, leaching temperature and leaching time were systematically investigated to achieve the highest leaching rate. For the electrodeposition process, the influences of Pb^{2+} concentration and $HClO_4$ concentration, temperature, current density, and additives on the electrode position process were studied in detail and optimized. The results show that the invented route has a lead leaching rate of above 98.5%, an electrolytic energy consumption of only 500 kWh $tonne_{Pb}^{-1}$, and a purity for the electrodeposited lead product of up to 99.9991%.

Keywords: Spent lead–acid battery; Leaching process; Electrodeposition; $HClO_4$

1. INTRODUCTION

Lead-acid batteries are one of the dominant batteries widely used in the fields of automobiles and energy storage because of advantages such as good temperature adaptability, low price, reliable performance, and high current charge-discharge [1-6]. In 2015, they accounted for 54.6% of the global market of secondary batteries, even if they are in fierce competition with lithium-ion batteries and nickel-hydride batteries [7-10]. It is thus urgent and important for developing an environmentally benign lead–acid industry to develop a clean, highly efficient lead recovery route with practical feasibility for recycling a huge amount of spent lead–acid batteries [11-13].

The main lead wastes of spent lead-acid batteries include spent lead paste and lead plate grids. The former consists of lead sulfate ($PbSO_4$), metallic lead, lead oxide (PbO), lead dioxide (PbO_2), and other impurities, such as Fe, Ba and Sn. The traditional pyrometallurgical lead recovery routes, including the Queneau - Schuhmann - Lurgi direct lead smelting process (QSL) [14], KIVCET direct lead smelting technology (Kivcet) [15], Shuikoushanlead smelting process (SKS) [16] and Oxygen enrichment top-blown smelting reduction technology of ISA-YMG [17], have many severe disadvantages, such as high energy consumption and lead pollution during the smelting process.

Recently, intense research has been conducted on the development of hydrometallurgical lead recovery routes, such as the solid phase electrolysis [18], RSR [19], CX-EW [20,21] and $PbCl_2$-NaCl-HCl [22] routes. The solid electrolytic route was a popular method from 1997–2007 for lead powders with direct recovery via one electrolytic process. However, the application of this method has been hindered by the high energy consumption (up to 760−950 kWh tonne_{Pb}^{-1}), time-consuming painting and solidification processes (a couples of days), incomplete reduction of $PbSO_4$ or PbO_2, and easy oxidation of the obtained super fine lead powders into PbO during the drying and melting processes. The RSR and CX-EW methods use a fluorosilicic acid (H_2SiF_6) solution in combination with desulfurated lead compounds to form H_2SiF_6-$PbSiF_6$ solutions, which are then electrolyzed to produce high purity metallic lead. H_2SiF_6 is a weaker acid with a lower ion conductivity than $HClO_4$, resulting in a higher electrolytic cell voltage (2.7-2.9 V) and energy consumption (810-930 KWh tonne_{Pb}^{-1}) during the electrolysis process [23-24]. In addition, H_2SiF_6 is easily decomposed into toxic HF and SiF_4 gases during the electrolysis process at temperatures of > 60 °C [25], potentially causing severe harm to operators and the environment.

A totally green hydrometallurgical lead recovery route via a H_2-PbO fuel cell has been recently reported by Pan et al. [26-27]. However, this new method is limited for industrial application due to the high cost of Nafion membranes and precious metal catalysts for the H_2 anode. Here, we report a novel, clean, highly efficient, and cost-effective hydrometallurgical lead recovery route with practical feasibility via a leaching–electrodeposition process in a perchloric acid ($HClO_4$) solution.

$HClO_4$ is a super strong acid with a higher solubility of Pb(II) compared with the methyl sulfonic acids H_2SiF_6 and HBF_4. It also has a high stability and ion conductivity because of the stable tetrahedron structure of ClO_4^-. With these merits, it is a very promising electrolyte for realizing a clean, highly efficient, and cost-effective hydrometallurgical lead recovery route [28-29].

Figure 1 shows a flow chart of the proposed new lead recovery route, which includes two processes as described below.

(1) Leaching process

In this process, desulfurated lead pastes and lead plate grids are converted into $Pb(ClO_4)_2$ via dissolution in the $HClO_4$ solution. The conversion includes the direct dissolution reaction of PbO and the redox reaction of Pb and PbO_2, as described by the reaction equations below.

$$Pb + PbO_2 + 4HClO_4 = 2Pb(ClO_4)_2 + 2H_2O \quad (1\text{-}1)$$

$$PbO + 2HClO_4 = Pb(ClO_4)_2 + H_2O \quad (1\text{-}2)$$

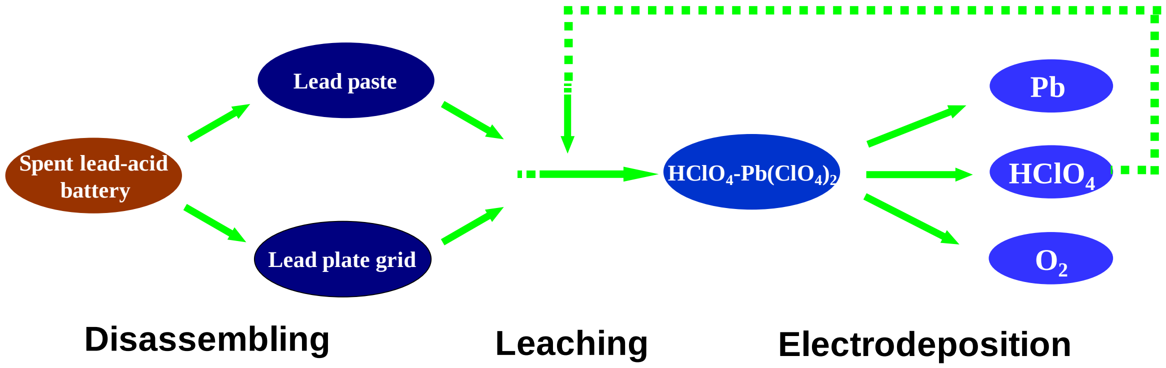

Figure 1. Flow chart of the leaching–electrodeposition of lead pastes and lead plate grids in perchloric acid ($HClO_4$) solution

(2) Electrodeposition process

In this process, high purity metallic lead is obtained from the aforementioned leaching solution of $HClO_4$-$Pb(ClO_4)_2$ via electrolysis, as described by the reaction equations below.

Cathode: $Pb^{2+} + 2e^{-} = Pb$ (2-1)

Anode: $H_2O - 2e^{-} = 1/2O_2$ (2-2)

Total reaction: $Pb(ClO_4)_2 + H_2O = Pb + 1/2O_2 + 2HClO_4$ (2-3)

The $HClO_4$ is regenerated, which can be easily reused during the leaching process for the next batch during the electrolytic process.

2. EXPERIMENT

2.1 Leaching process of the desulfurated lead paste and lead grid in the $HClO_4$ solution

The perchloric acid ($HClO_4$) (71 wt.%, industrial grade) was provided by Tianjin Xinyuan Chemical in China. The lead paste and lead plate grid were obtained from spent lead–acid batteries, as provided by the Zhejiang Chilwee Power Group, and their chemical compositions were measured using an ethylenediaminetetraacetic acid (EDTA) titration method [30].

The lead paste and lead plate grid were crushed (crusher, FW100, Tianjin Taisite Instrument) and then desulfurated in a NaOH solution. The obtained samples were filtered, and the filtered cake was washed with deionized water until the filtrate was neutral [30]. The desulfurated lead paste (100 g), spent lead plate grid (28 g), and $HClO_4$ solution (500 ml, 2.5 mol L^{-1}) were placed in a three-neck flask for leaching the lead with constant stirring at 30-60 °C in a water bath (DF-101S, Shanghai Kechuang Instrument). During the leaching process, the Pb^{2+} concentration and lead leaching rate were determined using an EDTA titration method [30].

2.2 Electrodeposition process in the $HClO_4$–$Pb(ClO_4)_2$ solution

The three-electrode battery system was subjected to cyclic voltammetry (CV) tests. The obtained $HClO_4$-Pb $(ClO_4)_2$ solution from the leaching process was used as the electrolyte, a refined copper plate (1 × 1 cm^2) was used as the working electrode, a platinum plate (2 × 2 cm^2) was used as the counter electrode, and a Hg/Hg_2SO_4 electrode was used as the reference electrode. The CV tests were performed on an electrochemical workstation (Shanghai CH Instruments) under a series of different Pb^{2+} concentrations, $HClO_4$ concentrations, and temperatures.

2.3 Electrolysis process in the $HClO_4$–$Pb(ClO_4)_2$ electrolyte

A copper plate (2 × 2.5 cm^2) was used as the current collector of the cathode, and a graphite plate (4 × 5 cm^2) or dimensionally stable anode (4 × 5 cm^2, Huaer-2#, Beijing Blue-Star Group) was used as the anode. The distance between the cathode and anode was kept at 2.0 cm. The obtained $HClO_4$-$Pb(ClO_4)_2$ solution, including additives of gelatin (1.0 g L^{-1}, Henan Haoda Electrochemicals Deposition Additives Group) and sodium lignin sulfonate (1.5 g L^{-1}, Henan Haoda Electrodeposition Additives Group), was used as the electrolyte. The galvanostatical electrolysis experiments were conducted on a LAND CT2001A cell test system (Wuhan Land).

2.4 Morphological and structural characterizations

The X-ray powder diffraction (XRD) patterns of the desulfurated lead paste and lead plate grid were collected using a Rigaku D/max 2500VB2+/PCX diffractometer with a Cu anticathode (40 kV, 200 mA) at a scan rate of 10° min^{-1} over a scan range (2θ) of 10° to 90°. The morphologies of the desulfurated lead paste, lead plate grid and the electrodeposited lead samples were examined using a field emission scanning electron microscope (FSEM, Hitachi S-4700). The contents of Pb and other elements in the electrodeposited lead were determined using an Inductively Coupled Plasma (ICP) analyzer (Agilent 7700).

3. RESULTS AND DISCUSSION

3.1 Leaching process

The FSEM images and XRD patterns of the crushed desulfurated lead paste and lead plate grid are shown in Figure 2. As shown in Figure 2a, the particle sizes of the crushed desulfurated lead paste were only approximately 300-400 nm. The small particle size provides a high contact area between the particles and $HClO_4$, which is beneficial for a quick lead leach by the reactions of Pb and PbO_2 particles in the $HClO_4$ solution. Figure 2b shows that the major diffraction peaks of the sample correspond to the characteristic peaks in the standard cards of PbO_2 (JCPDF#41-1492), α-PbO (JCPDF#85-1739), β-PbO (JCPDF#88-1589) and Pb (JCPDF#4-0686), indicating that the desulfurated lead paste mainly consists of Pb, PbO_2, and PbO. Figure 2c shows the FSEM image of the crushed desulfurated lead grid. In contrast to the paste, it primarily consists of metallic Pb, as verified by the XRD patterns shown in Figure 2d.

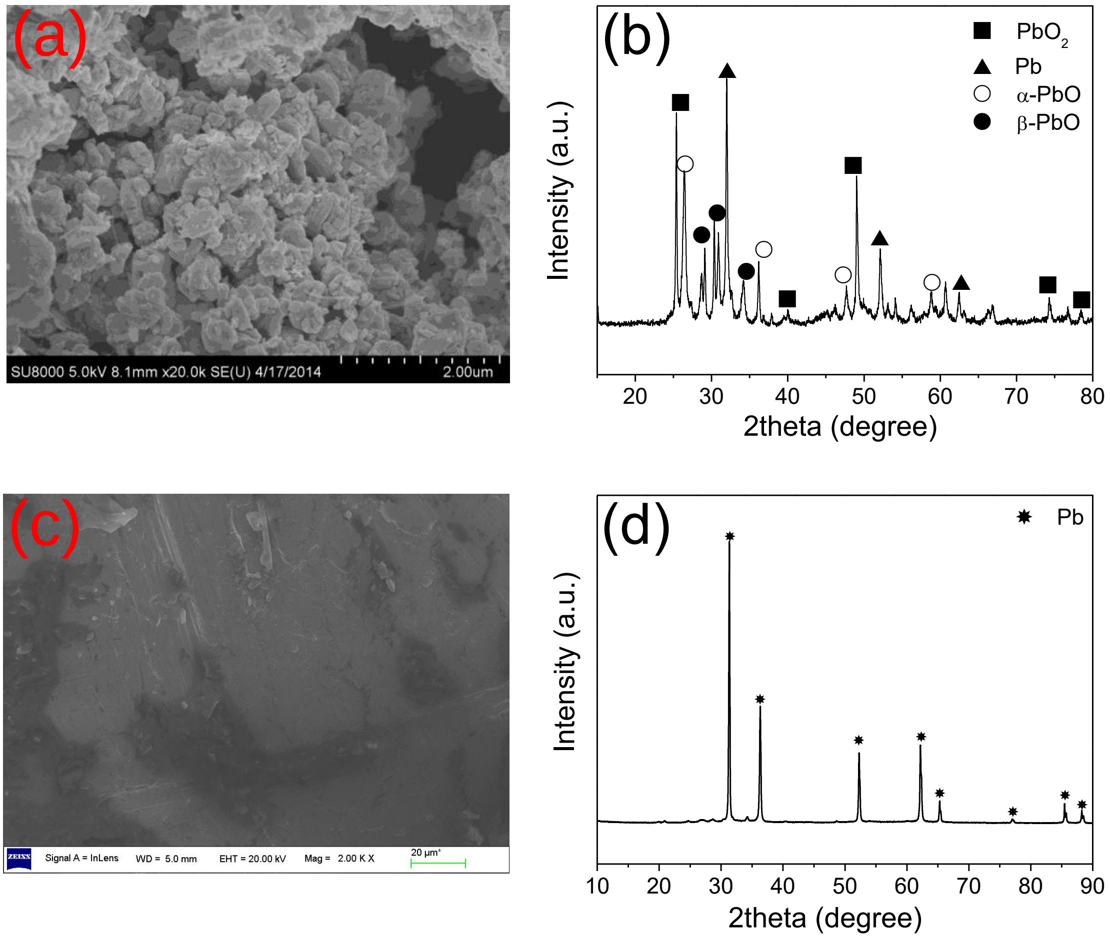

Figure 2. (a, c) FSEM images and (b, d) XRD patterns of (a, c) the lead paste and (b, d) the lead plate grid

Table 1. Chemical compositions of the desulfurated spent lead paste

			wt.%		
sample	PbO/%	Pb	$PbSO_4$	PbO_2	Others
1	42.36	11.07	0.09	46.11	0.37
2	42.16	11.22	0.10	46.21	0.40
3	42.44	11.09	0.07	46.05	0.35

Table 1 presents the chemical compositions of the desulfurated lead paste, as determined by the EDTA titration method. The results indicate that the lead paste primarily consists of 11.07 wt.% Pb, 46.11 wt.% PbO_2, and 42.36 wt.% PbO. The Pb and PbO_2 are synchronously generated by the charge process of lead-acid batteries. According to the stoichiometry of the reaction, the contents of metallic Pb and PbO_2 should be equivalent to the mole ratio, respectively. The deviation of their contents in the lead paste is attributed to the easy oxidation and sulfuration of the metallic Pb particles in the negative electrode by oxygen in the air and the sulfuric acid from the residue electrolyte, respectively, during the disassembly process of spent lead acid batteries. To dissolve the excessive stoichiometric amount of PbO_2, the lead plate grid was added as a clean reductant (with the amount calculated based on the composition in Table 1 and reaction stoichiometry) to react with PbO_2 to form PbO. As a result, the spend lead paste and lead grid are totally converted into $Pb(ClO_4)_2$ during the leaching process.

The influences of the $HClO_4$ concentration, reaction temperature, and reaction time on the lead leaching rate were also systematically investigated. Figure 3a shows the lead leaching rates at different concentrations of $HClO_4$.

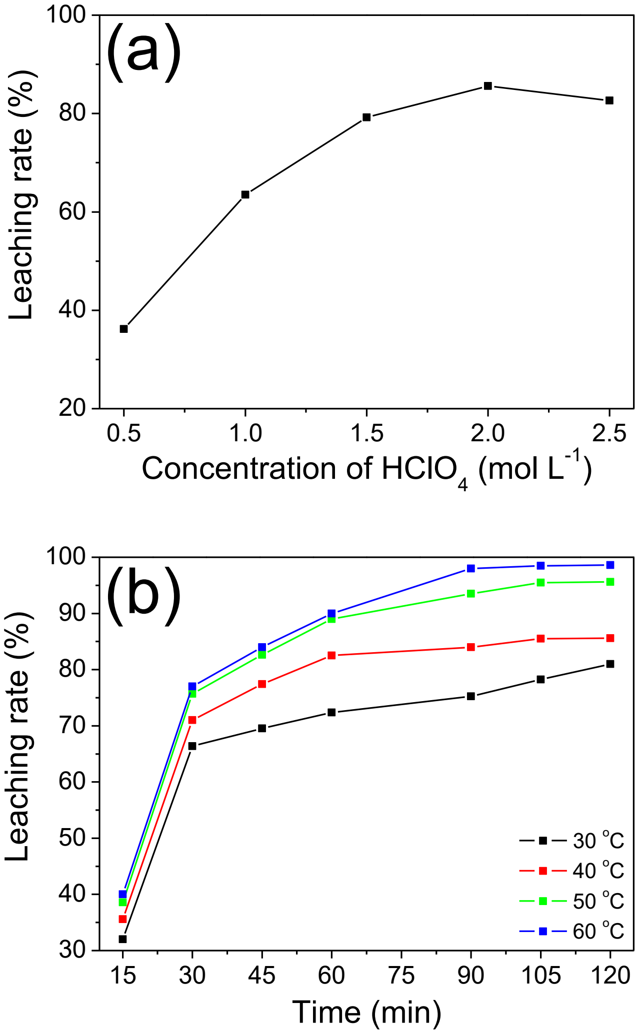

Figure 3. (a) Lead leaching rates for different concentrations of $HClO_4$ solutions at 40 °C for 2 h; (b) Curves of the lead leaching rate versus time in a 2.0 mol L^{-1} $HClO_4$ solution at different temperatures

The rate increased from 35% to 82% as the concentration of $HClO_4$ increased from 0.5 to 2.0 mol L^{-1}. This indicated that a high concentration of $HClO_4$ is beneficial for improving the lead leach speed during the leaching process. One reason might be that a high concentration of $HClO_4$ can promote the redox reaction of Pb and PbO_2, and the generated PbO can be quickly removed by the $HClO_4$ solution. As the concentration of $Pb(ClO_4)_2$ gradually approached the saturation value, the leaching rate tended to decrease. Thus, the leaching rate began to decline after the concentration of

$HClO_4$ was above 2.5 mol L^{-1}. Therefore, 2.0 mol L^{-1} was determined to be the optimal $HClO_4$ concentration for the leaching process.

Figure 3b displays curves for the lead leaching rate versus time at different temperatures from 30 to 60 °C. The leaching rate obviously increased with temperature during the first 90 min, and then the leaching rate increased slightly to 98.5% during the next 30 min. Thus, a high reaction temperature can improve the reaction rate because of a reduced activation energy and increased collision rate of Pb and PbO_2 particles. Increasing the temperature also accelerated the transformation of the reaction product of PbO. The reaction of Pb and PbO_2 and the dissolution of PbO in the $HClO_4$ solution are exothermic reactions. The heat generated promotes the reaction and dissolution as a chain effect. Thus, the leaching process should be conducted at an optimal temperature of 60 °C and at an optimal leaching time of 120 min. Compared with the leaching time of 5 h for the previously method [30], it was only 2h for the new method, much less than the former.

3.2 Electrodeposition process

Figure 4a presents the cyclic voltammetry curves for lead electrodeposition at different Pb^{2+} concentrations. A current loop phenomenon can be observed when the potential scans back during the positive scan process, which indicates that the surface area of the negative electrode increased by the deposited Pb during the negative scan process. As shown in Figure 4a, the cathodic reduction peak current was only 8.3 mA cm^{-2} at a Pb^{2+} concentration of 0.05 mol L^{-1}. With an increase of Pb^{2+} concentration from 0.05 to 0.50 mol L^{-1}, the reduction peaks current rapidly increased from 8.3 to 391.4 mA cm^{-2}. Compared with the reduction peaks current of 25 mA cm^{-2} in a NaCl - HCl system [22] and 60 mA cm^{-2} in HBF_4 - H_3BO_3 system [31], the higher current density in our $HClO_4$ system indicated that the reversibility of lead electrodeposition process was better than the existing systems. The peak position positively shifted by approximately 30 mV, indicating that the cathodic electrodeposition process became easier as the Pb^{2+} concentration increased. The electrodeposition process of Pb^{2+} is a typical lead diffusion controlled process; thus, an increased amount of Pb^{2+} is favorable for the electrolysis process.

The cyclic voltammetry curves in Figure 4b show the effects of $HClO_4$ concentration on the Pb^{2+} electrodeposition process. When the concentration increased from 0.5 to 2.0 mol L^{-1}, the reduction current rapidly increased from 57.2 to 79.1 mA cm^{-2}, and the reduction peak position also shifted from -0.74 to -0.68 V. This suggests that the increase in $HClO_4$ concentration not only enhanced the reduction current but also improved the electrochemical activity of Pb^{2+}. When the concentration reached 2.5 mol L^{-1}, a slight decrease in the reduction current was observed. Thus, the excessive amount of $HClO_4$ was not conducive to further improvement in the reduction current, and the optimum concentration of $HClO_4$ was 2.0 mol L^{-1}. Similarly, the same phenomenon was observed during the oxidation process of the electrodeposited lead.

The cyclic voltammetry curves in Figure 4c show the influences of temperature on the Pb^{2+} electrodeposition process. The reduction current of Pb^{2+} increased with temperature, and the reduction peak position also gradually shifted positively, implying that increasing the temperature of the electrolytes was beneficial for accelerating the electrochemical reduction rate of Pb^{2+}.

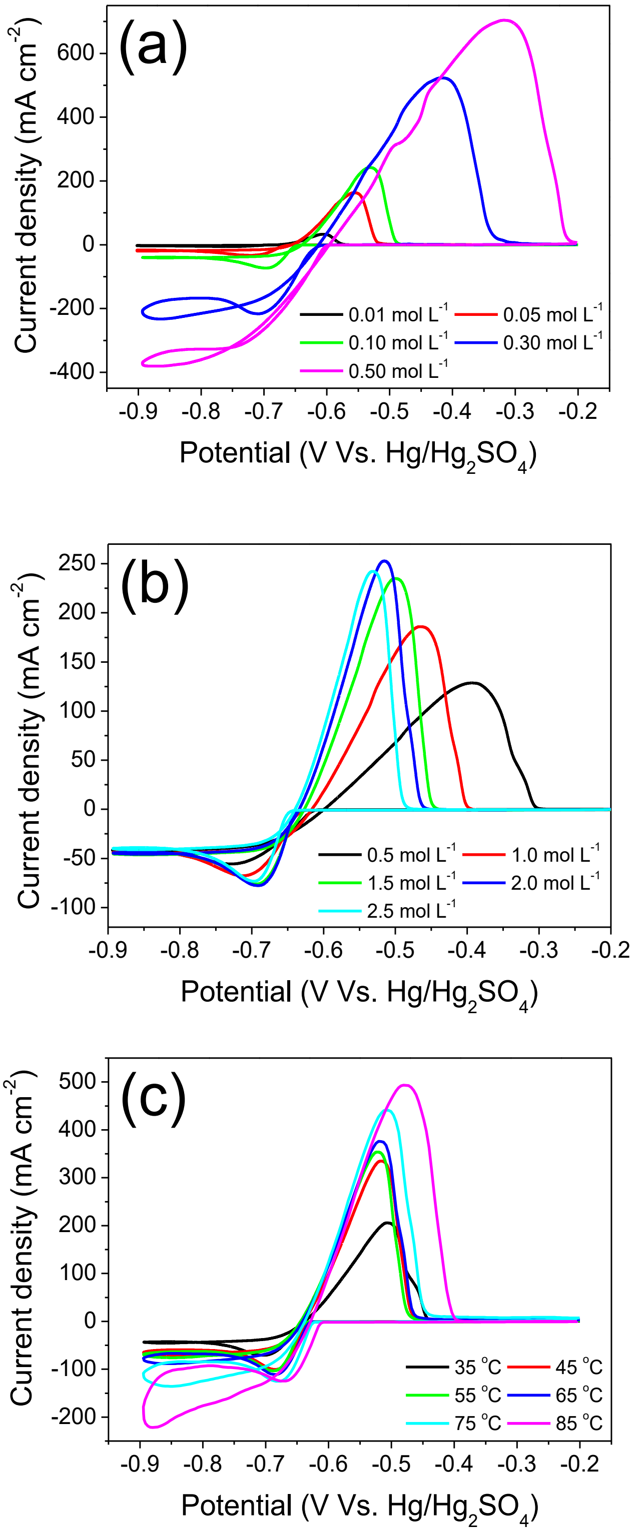

Figure 4. (a) Cyclic voltammetry curves for lead electrodeposition at different concentrations of (a) Pb^{2+} (scanning rate: 20 mV s^{-1}, concentration of $HClO_4$: 2.5 mol L^{-1}) and (b) $HClO_4$ (scanning rate: 20 mV s^{-1}, concentration of Pb^{2+}: 0.1 mol L^{-1}); (c) Cyclic voltammetry curves at different temperatures (scanning rate: 20 mV s^{-1}, concentration of $HClO_4$: 2.0 mol L^{-1}, concentration of Pb^{2+}: 0.1 mol L^{-1})

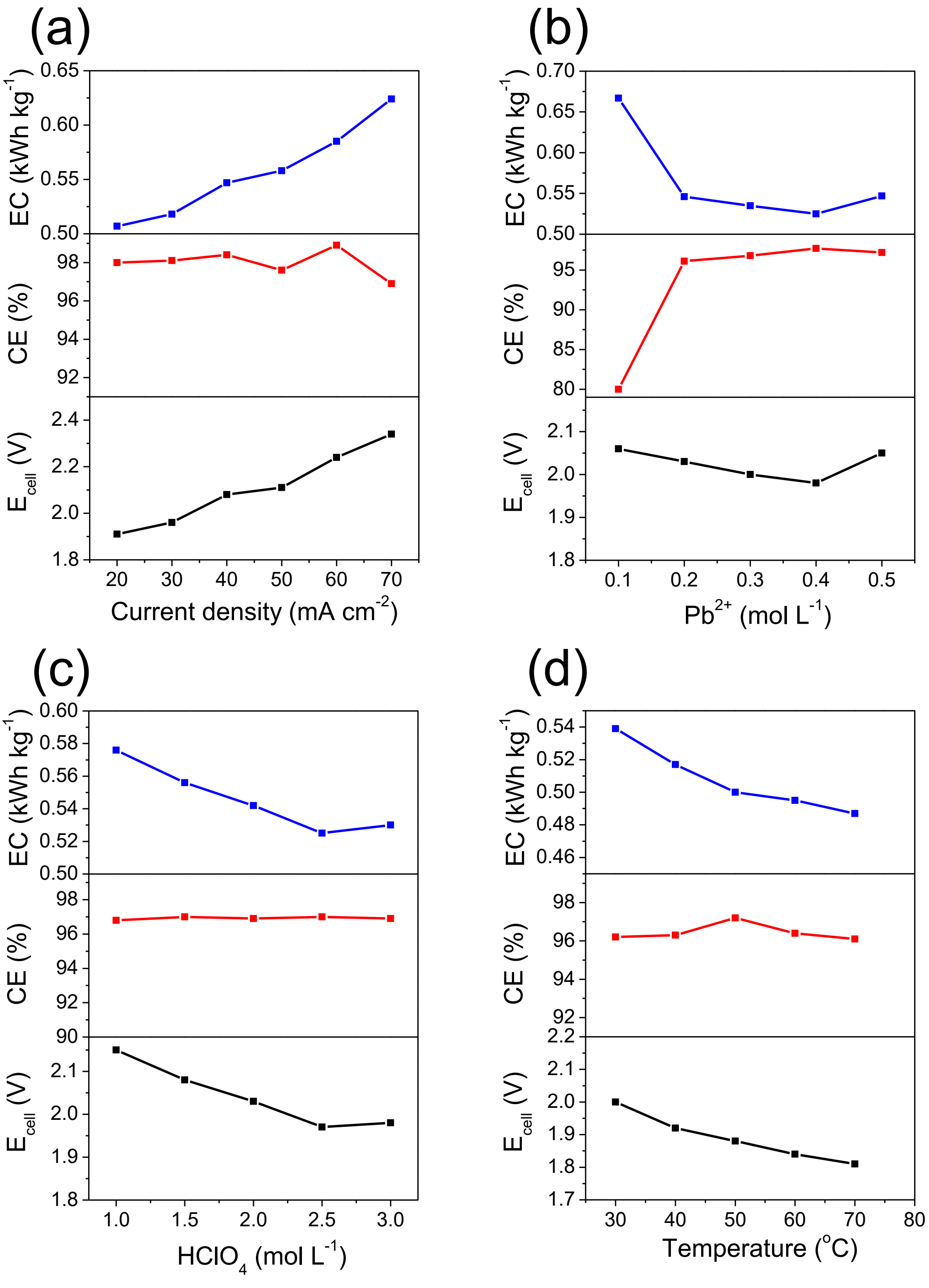

Figure 5. Cell voltages, current efficiencies and energy consumptions of the leaching–electrodeposition lead recovery route at different (a) current densities, (b) concentrations of Pb^{2+}, (c) concentrations of $HClO_4$, and (d) temperatures

Although the highest redox peak was observed at 85 °C, considering the rapid evaporation rate of water, corrosion of equipment, and energy consumption for heating the system, the optimal temperature for the electrodeposition process was determined to be approximately 65 °C. Compared with the RSR route [19], in which the temperature should be below 35 ^{o}C because H_2SiF_6 was easy to volatilize, leading to higher polarization of electrolysis reactions. However, the $HClO_4$ was a super strong acid without volatilization characteristics, even under higher operating temperature of 65°C which is more beneficial to reduce the polarization and its energy consumption [29].

The effects of current density, lead concentration, concentration of $HClO_4$, and electrolyte temperature on the cell voltage (E_{cell}), current efficiency (CE) and electrolytic energy consumption (EC) of the electrodeposition process were investigated. The current efficiency (CE) and electrolytic energy consumption (EC) were calculated as follows:

$$\mathrm{CE\%} = \frac{\text{Charge used for the deposit of lead}}{\text{Total charge passed}} \times 100$$

$$\mathrm{EC}(\frac{\mathrm{kWh}}{\mathrm{kg\ Pb}}) = \frac{5361.1E_{\mathrm{cell}}}{M_{\mathrm{Pb}}\mathrm{CE\%}}$$

where M_{pb} represents the molar mass of lead (223 g mol^{-1}). The cell voltage (E_{cell}), current efficiency (CE) and electrolytic energy consumption (EC) of the electrodeposition process at different current densities, Pb^{2+} concentrations, $HClO_4$ concentrations, and temperatures are presented in Figure 5.

As shown in Figure 5a, the requirements of cell voltage and energy consumption synchronously increase with current density. When the current density was controlled between 20 and 60 mA cm^{-2}, the current efficiency was maintained at approximately 98%. However, when the current density increased to 70 mA cm^{-2}, the current efficiency slightly decreased, which might have been limited by the diffusion process of Pb^{2+}. Thus, a high current density caused a rapid rise in cell voltage and a decline in the current efficiency. Therefore, the current density should be controlled between 20 and 60 mA cm^{-2}. The current density of 60 mA cm^{-2} is much higher than that of 10 and 18 mA cm^{-2} in the acid chloride medium [22] and in H_2SiF_6 system [21], respectively. It can be expected that the time-space yield of the new method will be at least 3 times of the traditional process.

Figure 5b shows the influence of the Pb^{2+} concentration on the electrodeposition processes. The current efficiency increased from 80% to 98% by increasing the Pb^{2+} concentration from 0.1 to 0.4 mol L^{-1}. And the cell voltage was at the minimum value of 1.97 V much lower than that of 4.2 V and 2.5-2.7V of the existing two methods. So, the higher current efficiency and lower electrolysis voltage lead to lower energy consumption than the existing methods [22, 33]. Accordingly, the energy consumption of the new method decreased to 529 kWh tonne$_{Pb}^{-1}$, which can be explained because an increase in the Pb^{2+} concentration is beneficial to the enrichment of Pb^{2+} ions near the cathode surface, resulting in a decrease in the concentration polarization and an increase in the Pb electrodeposition rate. However, an extremely high Pb^{2+} concentration can cause an increase in the dissolution resistance of the Pb anode, leading to a high polarization or cell voltage. Thus, the best Pb^{2+} concentration is 0.4 mol L^{-1} for the electrodeposition process. Under the optimal Pb^{2+} concentration, the current efficiency reached a maximum value of 98%, much higher than 90% and 94-95% in the acid chloride system [22] and H_2SiF_6 system [33], respectively.

Figure 5c displays the influences of the $HClO_4$ concentration on the electrodeposition process. The experimental results show that increasing the $HClO_4$ concentration is beneficial for improving the ion conductivity of the electrolyte, thus reducing the electrolytic cell voltage. When the concentration acid reached 2.5 mol L^{-1}, the cell voltage reached a minimum of 1.97 V. Additionally, the $HClO_4$ concentration had little influence on the current efficiency, which was maintained at approximately 97.1%. After evaluating the effects on the cell voltage and current efficiency, 2.5 mol L^{-1} $HClO_4$ is recommended as the best electrolyte.

Figure 5d shows the influences of temperature on the electrodeposition process. As shown in the figure, the polarization of the electrodeposition process was significantly reduced as the electrolyte temperature increased, leading to a linear decline in the cell voltage. In terms of current efficiency, we observed that the current efficiency was up to 97% at 50 °C. Considering the current efficiency, cell voltage, and energy consumption for maintaining the temperature of the electrolytic cell, the lowest power consumption of 492-496 kWh ton^{-1}(Pb) was observed by controlling the operating temperature at 50-60 °C, which was only 64%, 60%, 63% and 37.6% of the energy consumption for the existing solid phase electrolysis, RSR, CX-EW and HCl-NaCl methods, respectively.

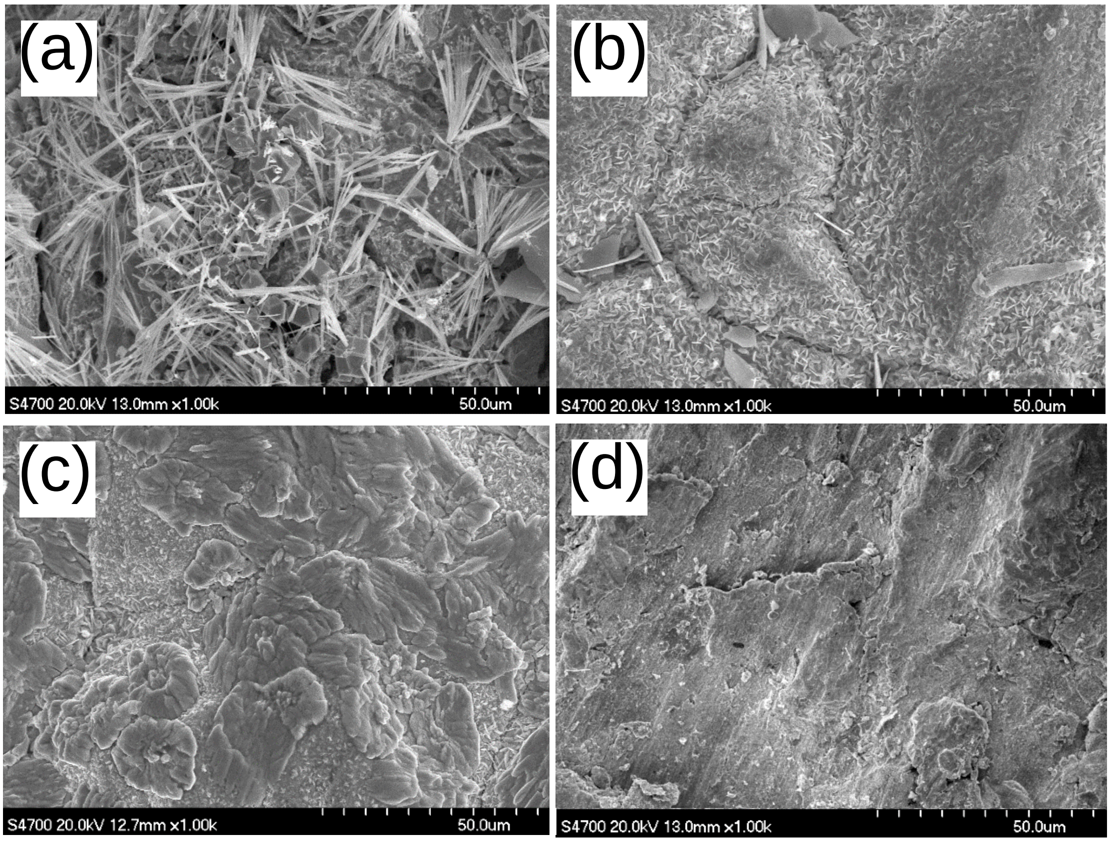

Figure 6. SEM images of the electrodeposited lead obtained (a) without additive and with an additive of (b) 1 g L^{-1} bone glue, (c) 1 g L^{-1} sodium lignosulfonate, or (d) 1 g L^{-1} bone glue and 1 g L^{-1} sodium lignosulfonate

Figure 6 shows the SEM images of the electrodeposited Pb samples obtained without and with different additives. As shown in Figure 6a, the Pb sample displayed many dendrites when no additive was added in the electrolyte. As electrolysis continued, these dendrites grew and/or fell off into the electrolyte, causing a short circuit between the two electrodes. Moreover, the Pb sample with many dendrites had a low density, and the dendrites were easier to oxidize via air than the bulk sample. The morphology of the obtained lead in $HClO_4$ system was denser than that of the deposition in HCl-NaCl solution without additives [22].

Table 2. ICP analysis results of the electrodeposited lead samples

	wt.%										
Sample	Sn	Sb	Bi	Cu	As	Ag	Zn	Cd	Ni	Fe	Pb
1	0.00005	0.00004	0.00012	0.00032	0.00001	0.00012	0.00006	0.00002	0.00002	0.00001	99.9992
2	0.00006	0.00016	0.00014	0.00033	0.00008	0.00010	0.00009	0.00005	0.00001	0.00001	99.9991
3	0.00010	0.00003	0.00014	0.00026	0.00013	0.00006	0.00012	0.00002	0.00003	0.00001	99.9991

When 1 g L^{-1} of bone glue or 1 g L^{-1} of sodium lignosulfonate was added, the surface of the electrodeposited Pb samples was relatively flat, as shown in Figures 6b and c. The additive of bone glue or sodium lignosulfonate can inhibit the growth of dendrites and improve the surface smoothness of electrodeposited Pb samples. A sample with a smoother surface is shown in Figure 6c, which was obtained when bone glue (1 g L^{-1}) and sodium lignosulfonate (1 g L^{-1}) were applied together during the electrodeposition process. The morphology of the obtained lead was more flat, more uniform and denser than that of in HCl-NaCl [22] and HBF_4 solution [33]. The Pb product without dendrites would achieve a maximal production rate by preventing the oxidation consumption during the casting process.

The ICP analysis results of the Pb sample shown in Table 2 show that the purity of the recovered Pb was up to 99.9991%, which was much higher than the 1# Pb of the Chinese national standard (GB/T 469-2013, purity of 99.994%) and PB990R of the European standard (EN 12659-1999, purity of 99.99%). Furthermore, the purity obtained by our method is up to 99.9991%, much higher than that by the solid phase electrolysis [14], RSR [15], CX-EW [16,17] and $PbCl_2$-NaCl-HCl [18] methods.

Table 3. Comparison of the new electrolytic process with the existing methods (Fluorine emission, the cell voltage (E_{cell}), energy consumption (EC) and lead purity)

Method	Fluorine emission (kg $tonne_{Pb}^{-1}$)	E_{cell} (V)	EC (kWh $tonne_{Pb}^{-1}$)	lead purity (%)	Reference
Solid phase electrolysis	0	2.2	950	99.994	[14]
RSR	4.2	2.7	930	99.994	[15]
CX-EW	4.2	2.6	910	99.99	[16,17]
$PbCl_2$-NaCl-HCl	0	4.2	1320	Not provided	[18]
Our method	0	1.9	492	99.9991	This work

A comparison between the properties of the previously reported methods [14-18] and our work is shown in Table 3. It is clear that there was no fluorine emission in our process while that in RSR and

CX-EW process reached up to 4.2 kg ton^{-1} (Pb). The energy consumption of our process is only 492 kWh tonne$_{Pb}$$^{-1}$, much less than that of the four methods.

All of the above results confirmed that the new process was a clean and energy saving recovery route for metallic lead in $HClO_4$ system.

4. CONCLUSION

The leaching rate of desulfurated spent lead paste was significantly improved by adding a spent lead grid as the reducing agent. Leaching experiments showed that an increase in $HClO_4$ is beneficial to promote the redox reaction of Pb and PbO_2, and the reaction is a typical exothermic reaction. Additionally, the reaction rate is great improved by increasing the reaction temperature. Optimization of the experimental conditions led to a leaching rate of the lead paste that was above 98.5% when the reaction time was 105 min, $HClO_4$ concentration was 2.0 - 2.5 mol L^{-1}, and leaching temperature was 60 °C.

CV experiments showed that the electrodeposition efficiency of Pb^{2+} in $HClO_4$ was affected by the concentrations of Pb^{2+} and $HClO_4$ and temperature. The optimal electrolysis conditions were as follows: the composition of the electrolyte was 2.0 mol L^{-1} $HClO_4$ + 0.4 mol L^{-1} Pb^{2+}, the additive was 1.0 g L^{-1} bone gel + 1.0 g L^{-1} sodium lignosulfonate at a current density of 20 mA cm^{-2}, and the temperature was 60-70 °C. Under these conditions, the current efficiency was greater than 97%, and for a cell voltage of 1.85 V, 492 kWh tonne$_{Pb}$$^{-1}$ Pb was achieved. The obtained electrodeposited lead with a flat morphology and purity of 99.9991% was higher than the Chinese national standard (GB/T 469-2013) and European standard (EN 12659-1999).

ACKNOWLEDGEMENT
This work was supported by the National Natural Science Foundation of China (21676022), the State Key Program of National Natural Science of China (21236003), and the Fundamental Research Funds for the Central Universities (JD1701, JD1612 & YS1406).

References

1. H. Y. Chen, S. Z. Duan, *J. Power. Sources*, 62 (1996) 213.
2. V. Kulhanek, *J. Power. Sources*,78 (1999) 2.
3. P. T. Moseley, D. A. J. Rand, B. Monahov, *J. Power. Sources*, 219 (2012) 75.
4. X. Tian, Y. Gong, Y. F. Wu, A. Agyeiwaa, T. Y. Zuo, *Resour. Conserv. Recy.*, 93 (2014) 75.
5. Z. Ghasemi, A. Tizpar, *Int. J. Electrochem. Sci.*, 2 (2007) 700.
6. A. Czerwinski, Z. Rogulski, S. Obrebowski1, J. Lach, K. Wrobel1, J. Wrobel1, *Int. J. Electrochem. Sci.*, 9 (2014) 4826.
7. N. L. N. Brenda, J. H. Li, B. Wilson, *J. Clean. Prod.*, 107 (2015) 237.
8. S. Matteson, E. Williams, *Energ. Policy*, 85 (2015) 71.
9. W. Fang, Y. L. Ma, P. J. Zuo, X. Q. Cheng, G. P. Yin, *Int. J. Electrochem. Sci.*, 8 (2013) 1949.
10. B. Pierozynski, *Int. J. Electrochem. Sci.*, 6 (2011) 860.
11. A. Zabaniotou, E. Kouskoumvekaki, D. Sanopoulos, *Resour. Conserv. Recy.*, 25(3-4) (1999) 301.
12. D. Andrews, A. Raychaudhuri, C. Frias, *J. Power. Sources*, 88 (2000) 124.

13. Z. Z. Wang, Q. T. Pei, *Resour. Recy.*, 5 (2008) 56.
14. P. Fischer, H. Maczek, *J. Miner. Met. Mater. Soc.*, 34(6) (1982) 60.
15. Y. Zhang, T. R. Meadowcroft, *Can. Metall. Quart.*, 43(2004) 395.
16. H. C. Wang, Z. M. Shi, T. Chen et al, *Nonferrous Metals*, (2011).
17. J. Wang, T. Zhou, G. Feng, *Eng. Sci.*, 6(4) (2004) 61.
18. K. H. Liu, L. I. Shu-Mei, Z. F. Cong, *Non-Ferrous Min. and Metall.*, 30(1) (2014) 32.
19. R. D. Prengaman, H. B. Mcdonald, (1980) *US4229271A[P]*.
20. M. Olper, P. Fracchia, (1988) *US4769116A[P]*.
21. Marco V. Ginatta, (1984) *US4451340[P]*.
22. E. Exposito, J. Iniesta, J. Gonzalez-Garcia, V. Montiel, A. Aldaz, *J. Power Sources*, 92 (2001) 260
23. J. A. González-Domínguez, E. Peters, D. B. Dreisinger, *J. Appl. Electrochem.*, 21(3) (1991) 189.
24. L. C. Ferracin, A. E. Chácon-Sanhueza, R. A. Davoglio et al, *Hydrometallurgy*, 65(2) (2002) 137.
25. D. Thomas, R. Olivier, C. Roderick, *Procedia Eng.*, 138 (2016) 231.
26. J. Q. Pan, Y. Z. Sun, W. Li, J. Knight, A. Manthiram, *Nat. Commun.*, 4 (2013) 2178.
27. A. Simon, H. Borrmann, *Angew. Chem. Int. Edit.*, 27(10) 1988 1339.
28. J. Q. Pan, C. Zhang, Y. Z. Sun, Z. H. Wang, Y. S. Yang, *Electrochem. Commun.*, 19 (2012) 70.
29. J. Q. Pan, X. Zhang, Y. J. Niu, Y. Z. Sun, (2012) CN201210031769.0[P].
30. J. Q. Pan, X. Zhang, Y. Z. Sun, S. Song, W. Li, P. Y. Wan, *Ind. Eng. Chem. Res.*, 55 (2016) 2059.
31. E. Exposito, J. Gonzalez-Garcia, P. Bonete, V. Montiel, A. Aldaz, *J. Power Sources*, 87 (2000) 137.
32. E. R. Cole, A. Y. Lee, D. L. Paulson, 1981 *US4272340[P]*.
33. Luiz C. Ferracin, Abel E. Chacon-Sanhueza, Rogerio A. Davoglio, Luis O. Rocha, Daniele J. Caffeu, Adilson R. Fontanetti, Romeu C. Rocha-Filho, Sonia R. Biaggio, Nerilso Bocchi. Hydrometallurgy 65 (2002) 137.